OPEN ACCESS
IOP Publishing
Superconductor Science and Technology
Supercond. Sci. Technol. **35** (2022) 054003 (11pp)
https://doi.org/10.1088/1361-6668/ac5fe3

Validation of a desktop-type magnet providing a quasi-microgravity space in a room-temperature bore of a high-gradient trapped field magnet (HG-TFM)

Keita Takahashi[1,*], Hiroyuki Fujishiro[2,*] and Mark D Ainslie[3]

[1] Department of Physics, Faculty of Science, Gakushuin University, 1-5-1 Mejiro, Toshima, Tokyo 171-8588, Japan
[2] Department of Physical Science and Materials Engineering, Faculty of Science and Engineering, Iwate University, 4-3-5 Ueda, Morioka, Iwate 020-8551, Japan
[3] Bulk Superconductivity Group, Department of Engineering, University of Cambridge, Cambridge CB2 1PZ, United Kingdom

E-mail: keita.takahashi@gakushuin.ac.jp and fujishiro@iwate-u.ac.jp

Received 4 February 2022, revised 11 March 2022
Accepted for publication 22 March 2022
Published 4 April 2022

Abstract

The concept of a high-gradient trapped field magnet (HG-TFM), which incorporates a hybrid system of two (RE)BaCuO superconducting bulk components with different functions, was proposed in 2021 by the authors based on the results of numerical simulations. The HG-TFM as a desktop-type magnet can be a more effective way to generate a higher magnetic field gradient product of $B_z \cdot dB_z/dz$ (>-1400 T^2 m^{-1}, as calculated for a pure water), which can realize a quasi-microgravity space applicable for Space Environment Utilization on a laboratory scale. In this study, to validate the quasi-microgravity space in the HG-TFM, a prototype HG-TFM apparatus has been built using a slit-bulk TFM and stacked full-TFM (without slits) with inner diameters of 36 mm. After field-cooled magnetization from 8.60 T at 21 K, a trapped field of $B_T = 8.57$ T was achieved at the center (i.e. at the bottom of a room temperature bore of 25 mm diameter outside the vacuum chamber), and consequently, a maximum $B_z \cdot dB_z/dz = -1930$ T^2 m^{-1} was obtained at the intermediate position between the slit-bulk TFM and the stacked full-TFM. Magnetic levitation was demonstrated successfully for bismuth particles and a pure water drop, which validates the quasi-microgravity environment in the HG-TFM. Based on numerical simulation results of the trapped field profile, it is concluded that the reason for the instability of the levitated targets is because of the repulsive magnetic force applied along the horizontal plane. The levitating state can be controllable, for example, by changing the operating temperature, which would allow objects to levitate statically along the central axis.

* Authors to whom any correspondence should be addressed.

Keywords: bulk superconductors, trapped field magnets, high gradient magnets, magnetic levitation, quasi-zero gravity, magnetic force, quasi-micrograviy

(Some figures may appear in colour only in the online journal)

1. Introduction

High magnetic fields and magnetic field gradients are key parameters for developing a magnet able to levitate diamagnetic materials such as water, human cells and common metals. This so-called magnetic levitation can be achieved in an equilibrium condition, where the magnetic levitation force is applied such that it counteracts Earth's gravitational force. In scientific research fields—for example, in the life/medical sciences for protein crystallization [1] and cell culture [2, 3]—such magnetic levitation can be utilized as a quasi-microgravity space without natural convection due to gravity. Various case studies exploiting a quasi-, or real, micro-gravity space have been reported in the International Space Station (ISS) for the purposes of academic research, science education and space business [4]. This research field is an important developing base relating to the so-called 'Space Environment Utilization,' led by the Japan Aerospace Exploration Agency and the ISS program that aims to develop innovative technologies for human living on Earth as well as on space.

The potential energy per unit volume, U, of a diamagnetic particle in a static external B-field can be expressed in terms of the total amount of the magnetic energy, U_M, and the gravitational energy, U_g [5, 6],

$$U = U_M + U_g = -\frac{1}{2\mu_0}(\chi_s - \chi_m)B^2 + (\rho_s - \rho_m)gz, \quad (1)$$

where μ_0 is the vacuum permeability, $B = \sqrt{B_x^2 + B_y^2 + B_z^2}$ is the magnitude of the magnetic field, g is the acceleration due to gravity, and z is the vertical position. χ_s and ρ_s are the volume susceptibility and the density of the target substance, respectively. In the same sense, χ_m and ρ_m are the parameters for the medium surrounding the target, such as a liquid or gas. The total force density balance, F_z, along the z-direction (central vertical axis) at $x = y = 0$ mm, is given as,

$$F_z = -\frac{\partial U_{(x=y=0)}}{\partial z} = \frac{(\chi_s - \chi_m)}{\mu_0} B_z \frac{\mathrm{d}B_z}{\mathrm{d}z} - (\rho_s - \rho_m)g. \quad (2)$$

Hence, the magnitude of F_z is determined by the $B_z \cdot \mathrm{d}B_z/\mathrm{d}z$ value, the magnetic field gradient product, which changes depending on the position in the vertical bore of the levitation magnet. In the levitating condition, where the vertical component of the magnetic repulsive force is equivalent to the force of gravity, the equilibrium condition for magneto-Archimedes levitation can then be solved as,

$$B_z \frac{\mathrm{d}B_z}{\mathrm{d}z} = \frac{\rho_s - \rho_m}{\chi_s - \chi_m}\mu_0 g. \quad (3)$$

This relationship requires a large $B_z \cdot \mathrm{d}B_z/\mathrm{d}z$ value to levitate any substances with a small χ_s (>-1400 $\mathrm{T^2\ m^{-1}}$, as calculated for pure water by equation (3) and this is difficult to achieve using a conventional permanent magnet or electromagnets. Up to now, a large magnetic field sufficient for magnetic levitation can be generated by large-scale magnets: superconducting magnets (SMs), which can generate $B_z \cdot \mathrm{d}B_z/\mathrm{d}z$ up to -500 $\mathrm{T^2\ m^{-1}}$ with 10 T [7], and hybrid magnets with $B_z \cdot \mathrm{d}B_z/\mathrm{d}z$ up to -3000 $\mathrm{T^2\ m^{-1}}$ with 20 T [8]. A cryocooled 10 T SM is more practical on the laboratory scale from the viewpoint of its reasonable footprint, and it does not require any cryogenic coolants such as liquid nitrogen or liquid helium for operation. Hence, in most studies relating to magnetic levitation [7, 9] or magnetic separation [10, 11], the magneto-Archimedes method has been employed as to reduce the required $B_z \cdot \mathrm{d}B_z/\mathrm{d}z$ for magnetic levitation of a specific target by exploiting an additional paramagnetic gas or liquid (e.g. oxygen or aqueous $MnCl_2$). In this sense, there is a major difficulty in developing a practical magnet that improves magnetic performance and achieves this with a reasonable footprint; hence, providing a quasi-microgravity space in an efficient way.Large, single-grain (RE)BaCuO bulk superconductors (RE: rare earth element or Y) can be used as a so-called trapped field magnet (TFM) that can provide the trapped field after it is magnetized. In the field-cooled magnetization (FCM) process, for example, where an external magnetizing field is ramped down at a constant temperature below the superconductor's critical temperature, a magnetic flux density as large as several Tesla becomes trapped inside the material due to the 'vortex pinning effect', and the induced supercurrent flows with zero resistance quasi-permanently. Based on the critical state model reported by Bean [12, 13], the magnitude of the trapped field at the center of the top surface, B_T, of a disc-shaped bulk TFM can be expressed by,

$$B_\mathrm{T} = k\mu_0 J_\mathrm{c} a, \quad (4)$$

$$k = \frac{t}{2a}\ln\left(\frac{a}{t} + \sqrt{1 + \left(\frac{a}{t}\right)^2}\right), \quad (5)$$

where J_c is the critical current density of the superconducting material, a is the sample radius. k is a geometric factor to account for the finite thickness of the disc bulk, t [14]. Hence, based on equation (4), a simple way to achieve a higher $B_z \cdot \mathrm{d}B_z/\mathrm{d}z$ for magnetic levitation is to achieve a higher B_T by improving the superconducting properties (i.e. J_c) or enlarging the diameter of the material. The record-high trapped field of 17.6 T was achieved at the center of a stacked disc-shaped GdBaCuO bulk pair magnetized by FCM with an external field of 17.8 T at 26 K using stainless steel (SS) rings for mechanical reinforcement [15]. In subsequent experiments, it was confirmed that laminated structures exploiting SS spacers within the stacked bulks are more reliable for realizing similar B_T values over 17 T [16].

To develop a practical magnet using bulk superconductors from the viewpoints of both the $B_z \cdot dB_z/dz$ performance and the magnet versatility (e.g. easy to operate on a laboratory scale), the authors proposed a new concept of hybrid-type TFMs which incorporates two bulk components with different functions: a hybrid trapped field magnet lens (HTFML) and a high gradient trapped field magnet (HG-TFM). In the numerical simulations of the HTFML in 2018 [17], a concentrated magnetic field, $B_c = 11.0$ T, was obtained owing to the diamagnetic lens effect of the inner bulk lens magnetized by the zero field-cooled magnetization (ZFCM) process, which is higher than the trapped field from the outer bulk TFM cylinder magnetized by FCM in the descending stage of the ZFCM process with 10 T at 40 K. A maximum $B_c = 9.8$ T was validated in experiments with a 7 T external field exploiting a loose contact method [18], where a huge temperature difference between each bulk component, as large as $\sim$100 K, was realized to incorporate two magnetizing processes: FCM of the outer bulk cylinder and ZFCM of the inner magnetic bulk lens, systematically. In contrast, the HG-TFM, which incorporates slitted ring bulks stacked on a conventional bulk cylinder, has the advantage of improving the field gradient, dB_z/dz, by controlling the trapped field profile with an inverted field from the slit-bulk. Numerical results showed that a maximum value of $B_z \cdot dB_z/dz = -6040$ T^2 m^{-1} was estimated in the case of the HG-TFM with an inner diameter (I.D.) of 10 mm magnetized by FCM with 10 T at 40 K [19]. This suggests a more effective way for magnetic levitation since the HG-TFM requires just a simple FCM process at a constant temperature and can provide a higher $B_z \cdot dB_z/dz$ value in an open space outside the vacuum chamber.

In this study, to validate the quasi-microgravity space in the HG-TFM, we have built a prototype device using a slit-bulk TFM and stacked full-TFM (without slits) with I.Ds. of 36 mm. This results in a room temperature bore of 25 mm diameter. All of bulk components are encapsulated in a SS capsule for reinforcement and tightly connected to the cold stage of the cryocooler for cooling (before magnetization) to the lowest temperature of 21 K. In the present HG-TFM, a trapped field at the center (i.e. the bottom of the room temperature bore outside the vacuum chamber) of $B_T = 8.57$ T was achieved by FCM from 8.60 T at 21 K, and consequently, a maximum $B_z \cdot dB_z/dz = -1930$ T^2 m^{-1} was obtained at the intermediate position between the slit-bulk TFM and the stacked full-TFM. Magnetic levitation was demonstrated for bismuth particles and a pure water drop in the room temperature bore of the HG-TFM. Numerical simulation of the trapped field profile was also carried out to explain the instability of the levitated targets observed by an optical microscope in the experiment.

2. Experimental setup

Figure 1(a) presents the cross-sectional schematic view of the experimental setup of the HG-TFM, in which a stack of ring-shaped TFM cylinders, labeled 'full-TFM,' is attached to a separate TFM cylinder with two slits 500 μm in width, labeled 'slit-TFM'. Figures 1(b) and (c), respectively, show the top views of the full-TFM and slit-TFM. The outer diameter of the HG-TFM is 60 mm and the I.D. is 36 mm. All of these bulk superconductors were fabricated by using the QMG^{TM} method (Nippon Steel Corporation, Japan) and each bulk was machined mechanically to prepare each of the full-TFM and the slit-TFM part of the HG-TFM. The total height (H) of the three stacked full-TFM components is 60 mm (each 20 mm in H), and the single, slit-TFM is 17 mm in H. Note that a SS spacer of 1 mm in H is necessary to isolate the magnetic loop of each bulk component. All of the bulk materials are encapsulated in an Al alloy ring 5 mm in thickness and a SS holder 5 mm in thickness for mechanical reinforcement, as shown in figure 1(a). The numerical assumptions for the mechanical reinforcement were discussed previously in the conceptual paper [19], in which a compressive stress of -100 MPa provided by both the Al-alloy rings and the SS capsule with a cooling process from 300 K to 40 K would be enough to counteract the electromagnetic hoop stress of about 100 MPa during FCM from an applied field of 10 T. In the present experiment, in which a temperature gradient would occur across such large, four-stacked TFMs of $\approx$100 mm in total height H, a copper heat sink is also incorporated for achieving better cooling from the inner periphery of each TFM. Overviews of the whole apparatus are also presented in the photographs in figure 2. The outer size of the apparatus including the cryocooler is (35 cm $\times$ 35 cm) $\times$ 103 cm in height, which includes a room-temperature bore of 25 mm in diameter and 80 mm in depth.

The temperature was monitored on the top surface of the outer SS capsule using a Cernox^{TM} thermometer and under the cold stage of the 10 K GM-cycle helium cryocooler using a Pt–Co thermometer (for details, see section 4). The HG-TFM was enclosed in a vacuum chamber, in which an ambient pressure was kept below 10^{-3} Pa using a turbo-molecular pump. A cryocooled 10 T SM (JASTEC, JMTD-10T100) was used to magnetize the HG-TFM by FCM from an applied field of 8.60 T, which was ramped down at a constant rate of -0.05 T min^{-1}. It was predicted for the HG-TFM that an applied field above 8 T would be enough to achieve the required $B_z \cdot dB_z/dz$ value as large as -1400 T^2 m^{-1} for magnetic levitation of pure water [19]. During the magnetizing process, the trapped field was measured using an axial-type Hall sensor at $z = 0$ mm, the bottom of the room-temperature bore corresponding to 2 mm above the center of the full-TFM component. Hence, the interface of the two bulk components between the slit-TFM and the full-TFM is at $z = 28$ mm. The external magnetic field was calculated from the electric current measured by a shunt resistor. The fundamental diamagnetic targets—bismuth particles and a pure water drop—are levitated in the room-temperature bore outside the vacuum chamber to demonstrate the quasi-microgravity space in the HG-TFM. The *in-situ* observation of magnetic levitation was carried out using an optical microscope system (OLYMPUS Ltd, MK027) connected to a CCD camera. Material properties, including the density and the volume susceptibility, were measured using a magnetic balance (Sherwood Scientific Ltd, MSB-MKI) for theoretical calculations using equation (3).

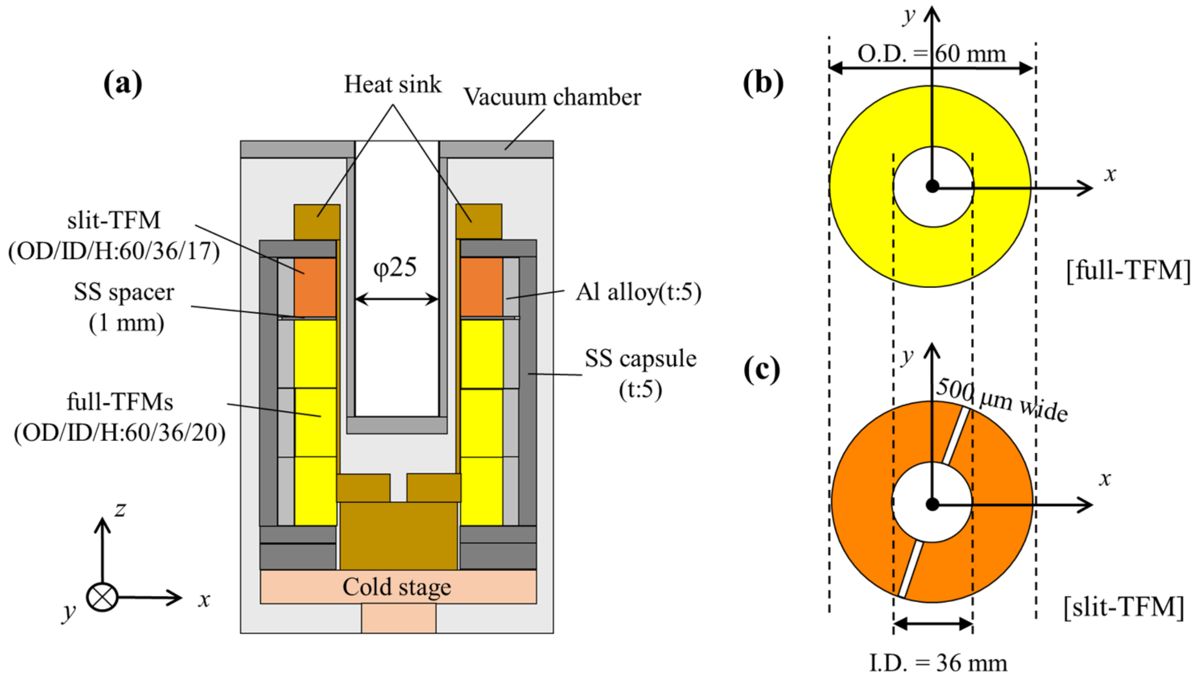

Figure 1. (a) Cross-sectional schematic view of the experimental setup of the HG-TFM, in which a stack of three conventional ring-shaped TFM cylinders, labelled 'full-TFM' (yellow), is attached to a separated TFM cylinder with two slits 500 μm in width, labelled 'slit-TFM' (orange). The top views of the full-TFM and slit-TFM are also shown in (b), (c), respectively.

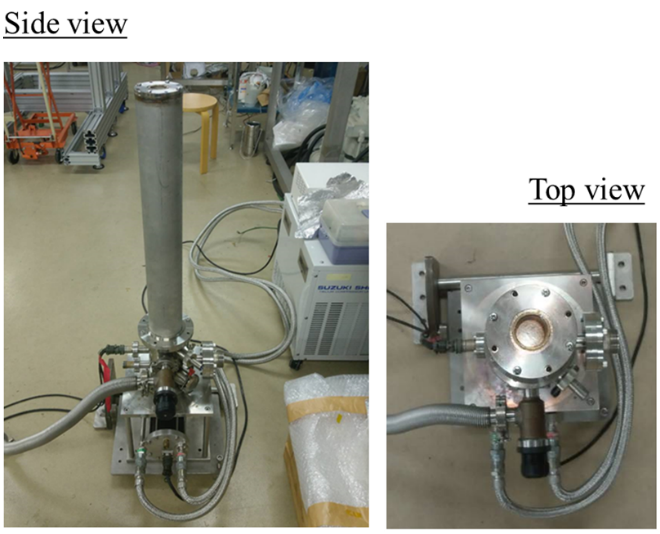

Figure 2. Side and top views of the whole apparatus. The outer size of the apparatus is (35 cm × 35 cm) × 103 cm in height, which includes a room-temperature bore of 25 mm in diameter and 80 mm in depth.

3. Numerical modelling framework

Based on the experimental setup shown in figure 1, a three-dimensional (3D) numerical model of the HG-TFM was constructed using the commercial software Photo-EDDY (Photon Ltd, Japan), in which the magnetization of the HG-TFM by the external SM was resolved using the finite element method [20–22]. The simulation procedure and the superconducting parameters used in the present modeling were also described previously in the original numerical study of the HG-TFM [19].

The nonlinear E–J characteristic of the bulk superconductor is represented by a power-n law as follows,

$$E = E_c \left(\frac{J}{J_c}\right)^n, \tag{6}$$

where E_c ($=10^{-4}$ V m^{-1}) is the characteristic electric field, and $n = 20$ is a typical value for (RE)BaCuO bulk superconductors [23, 24]. The critical current density, $J_c(B)$, can be described by the following equation reported by Jirsa *et al* [25–27],

$$J_c(B) = \beta \cdot \left\{ J_{c1} \exp\left(-\frac{B}{B_L}\right) + J_{c2}\frac{B}{B_{max}} \times \exp\left[\frac{1}{\alpha}\left(1-\left(\frac{B}{B_{max}}\right)^{\alpha}\right)\right]\right\}, \tag{7}$$

where each fitting parameter, J_{c1}, B_L, J_{c2}, B_{max}, and α can be determined from a realistic experimental J_c value. The fitting coefficient, β, was also introduced to reproduce the actual trapped field value in experiments, as reported in [28], but for 20 K in the present simulation. The fitting parameters for bulk superconductors used in equation (7) are presented in table 1.

There is a minor discrepancy between the numerical model and the experimental setup shown in figure 1, for which the slit-TFM has a wider slit, 6 degrees wide, due to a limitation of the number of mesh elements required. Note that the other non-superconducting components in the HG-TFM (Al alloy,

Table 1. Numerical fitting parameters for the assumed $J_c(B)$ characteristics of the GdBaCuO bulk for equation (7), where the β value is adjusted to reproduce the experimental result for the trapped field by FCM at 20 K.

T (K)	J_{c1} (A m^{-2})	B_L (T)	J_{c2} (A m^{-2})	B_{max} (T)	α	β
20	9.0×10^9	1.5	5.4×10^9	8.0	0.5	0.29

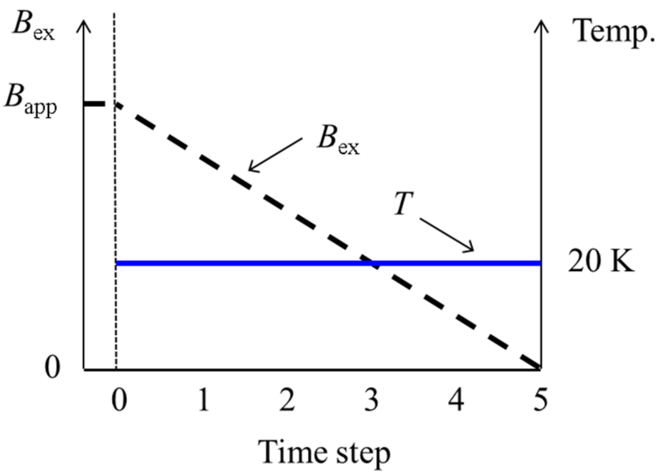

Figure 3. Time sequence of the external field, B_{ex}, at the center of the magnetizing solenoid coil, and the operating temperature, T, during FCM of the HG-TFM in the simulation. The applied field, B_{app}, corresponding to the initial B_{ex} value, was ramped down from 8.60 T to 0 T over six steps with a ramp rate of -0.05 T min^{-1}. The temperature, $T = 20$ K, was assumed to be constant and uniform, assuming isothermal conditions.

SS and copper) were considered as a non-magnetic material (assumed as air) for the present FCM process that is essentially quasi-static with a slowly-ramped magnetic field.

Figure 3 presents the conceptional view of time sequence of the external field, B_{ex}, at the center of the magnetizing solenoid coil and the operating temperature, T, during FCM of the HG-TFM in the simulation. The applied field, B_{app}, corresponding to the initial B_{ex} value, was ramped down from 8.60 T to 0 T over six steps with a ramp rate of -0.05 T min^{-1}. The temperature, $T = 20$ K, was assumed to be constant and uniform, assuming isothermal conditions.

4. Experimental results

Figure 4 shows the typical experimental results of the cooling test, for which the temperatures were measured on the top surface of the HG-TFM, T_{top}, and under the cold stage, T_{stage}. Note that the magnetizing process is not yet included in this initial stage. The temperature was cooled down from 300 K and reached the lowest values 10 h later: $T_{stage} = 17.5$ K under the cold stage and $T_{top} = 21.0$ K at the top surface of the HG-TFM. Hence, the temperature difference between each measurement point was minimized to within 4 K owing to the utilization of the copper heat sink. The use of this heat sink is recommended to achieve better cooling efficiency for such stacked TFM cylinders.

Figure 5 shows the time dependence of (a) the temperatures measured at each position, and (b) the external field, B_{ex}, and the magnetic field, B_z, during magnetization with an applied field, $B_{app} = 8.60$ T. During magnetization, the temperatures gradually increased with decreasing external field and T_{top} took a maximum value of 54.9 K. Such thermal instability may cause flux jumps and mechanical fracture of the bulk cylinder; hence, the temperature should be kept as constant as possible. In the present setup, a trapped field as large as $B_T = 8.57$ T can be maintained without flux creep even after completing the magnetization process. This implies that the stacked TFM cylinders could have sufficient capability in terms of their critical current density for partial magnetization with $B_{app} = 8.60$ T at a relatively high temperature above 50 K for FCM, where the induced current might flow around the outer peripheral region and not saturate inside of each of the TFMs.

Figure 6(a) shows the magnetic field, B_z, and the magnetic field gradient product, $B_z \cdot dB_z/dz$, profiles measured by scanning a Hall probe inside the room-temperature bore of the HG-TFM along the z-direction after FCM from $B_{app} = 8.60$ T at 21 K. A schematic view of the apparatus that includes the optical observation system for magnetic levitation is also presented. It is shown that the maximum peak value of $B_z \cdot dB_z/dz = -1930$ T^2 m^{-1} occurs at $z = 25$ mm, just below the interface of the two bulk components, between the slit-TFM and the full-TFM, and a trapped field $B_T = 8.57$ T is obtained at $z = 0$ mm, the bottom of the room temperature bore. Figure 6(b) shows photographs of the levitated targets: bismuth particles enclosed in a test tube, and a pure water drop, which is dripped from the tip of a dropper in air. The results of the *in-situ* observation can be download online (URL1: https://imgur.com/QSBNlF5, URL2: https://imgur.com/KX07NtE). Firstly, the levitated bismuth particles appear stable and collide with the counter side of the test tube against the camera, which floated at $z \cong 35$ mm (± 1 mm): here $B_z \cdot dB_z/dz = -695$ to -950 T^2 m^{-1}, obtained from the $B_z \cdot dB_z/dz$ profile in figure 6(a). On the other hand, the water drop moves up and down unstably because of gravity acceleration when it dripped out from the tip of the dropper. Meanwhile, the water drop was pushed out and collided with the side wall of the inner bore at $z \cong 30$ mm (± 1 mm): here $B_z \cdot dB_z/dz = -1308$ to -1595 T^2 m^{-1}. Comparing these materials, it is important to note that the magnetic buoyancy force along the z-direction should be applied slowly or step by step to levitate stably at a constant z-position as shown for the bismuth particles. This is difficult for a pure water drop in liquid form as it is. As for the stability along the horizontal plane, there is a common issue that both targets could not remain along the central axis, $x = y = 0$ mm, due to a repulsive magnetic force along the

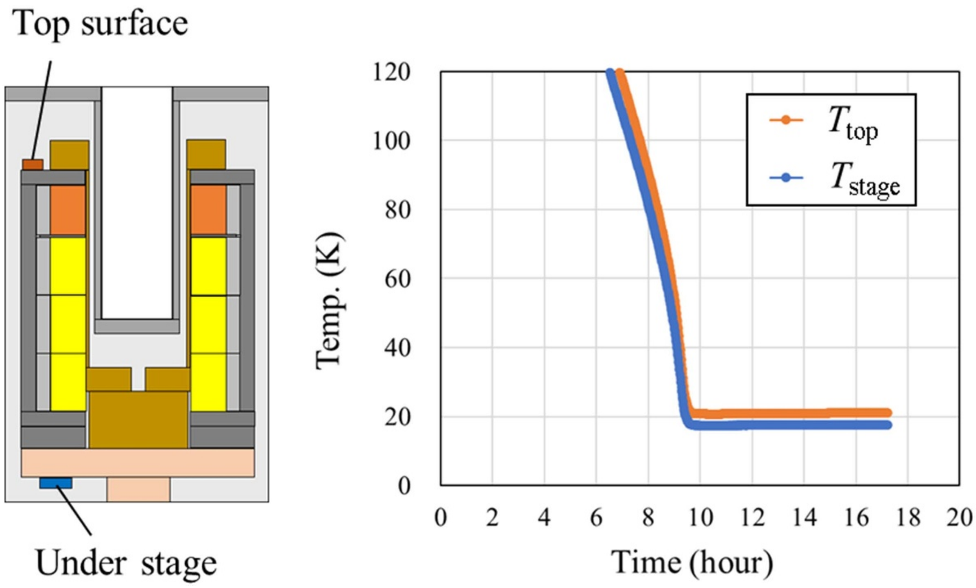

Figure 4. Typical experimental results for the cooling test, for which the temperatures were measured on the top surface of the HG-TFM, T_{top}, and under the cold stage, T_{stage}. Note that the magnetizing process is not yet included in this initial stage.

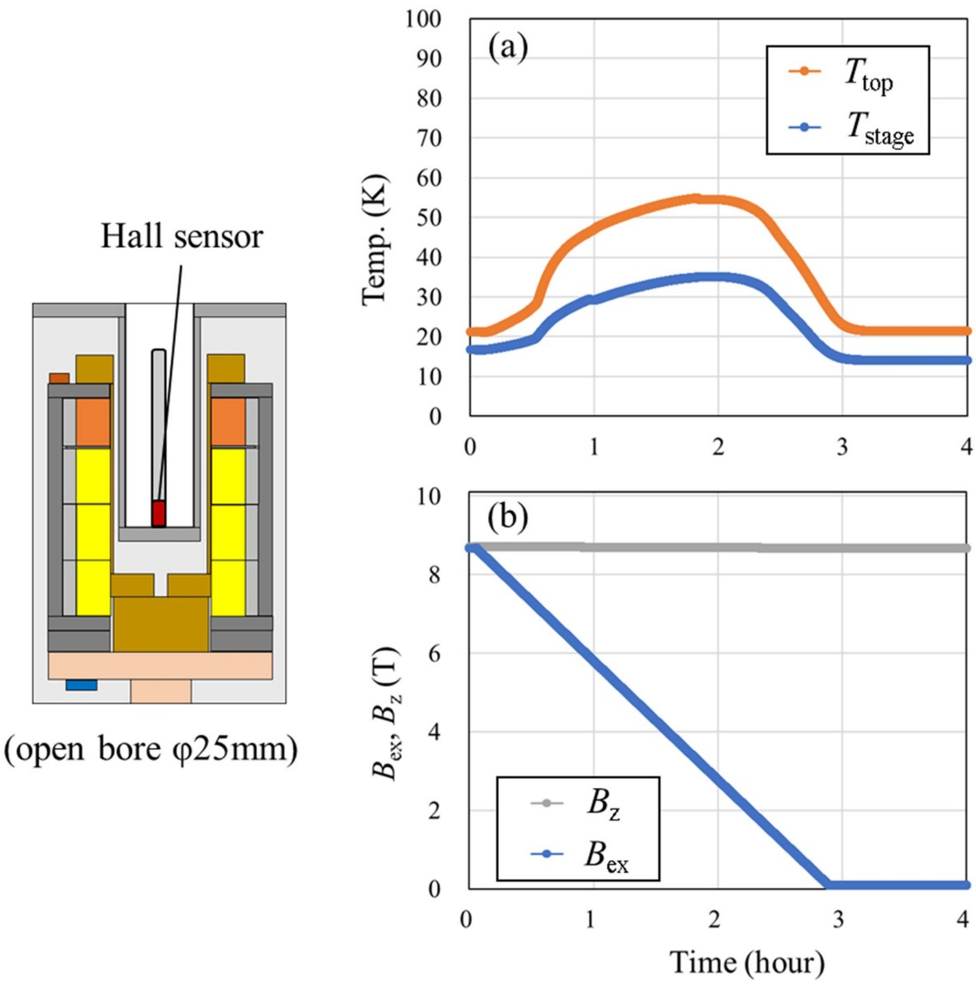

Figure 5. (a) Time dependence of the temperatures measured at each position, and (b) the external field, B_{ex}, and the magnetic field, B_z, during magnetization with an applied field, $B_{app} = 8.60$ T. A Hall probe is placed on the bottom of the room-temperature bore, which corresponds to the center of the external SM.

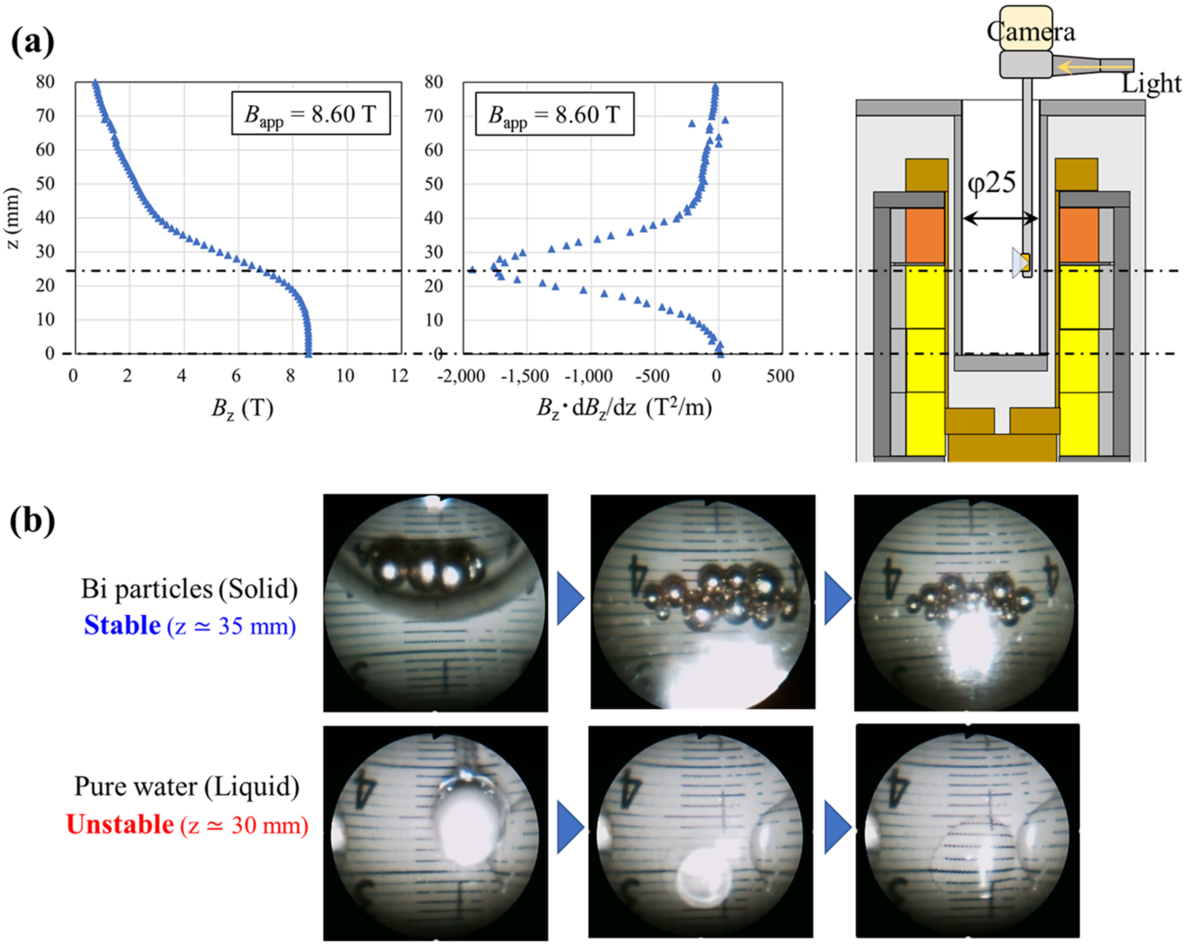

Figure 6. (a) The magnetic field, B_z, and the magnetic field gradient product, $B_z \cdot dB_z/dz$, profiles measured by scanning a Hall probe inside the room-temperature bore of the HG-TFM along the z-direction after FCM from $B_{app} = 8.60$ T at 21 K. A schematic view of the apparatus that includes the optical observation system for magnetic levitation is also presented. (b) Photographs of the levitated targets: bismuth particles enclosed in a test tube, and a pure water drop, which is dripped from the tip of a dropper in air. The results of the *in-situ* observation can be downloaded online (URL1: https://imgur.com/QSBNlF5, URL2: https://imgur.com/KX07NtE).

Table 2. Material properties of density, ρ_s, and the volume susceptibility, χ_s, as well as the calculated $B_z \cdot dB_z/dz$ values compared with the experimental $B_z \cdot dB_z/dz$ values obtained from the corresponding levitation positions.

Targets	Density ρ_s (g cm^{-3})	Volume susceptibility χ_s (-, SI)	Calculated $B_z \cdot dB_z/dz$ (T^2 m^{-1})	Experimental $B_z \cdot dB_z/dz$ (T^2 m^{-1})
Bismuth	3.54	-4.93×10^{-5}	−879	−695 to −950
Pure water	0.995	-8.54×10^{-6}	−1376	−1308 to −1595

horizontal plane, which will be discussed later based on the numerical results shown in figure 8. These experimental results validate that the present HG-TFM can provide a quasi-microgravity space, where a buoyancy magnetic force along the z-direction is sufficient to levitate the target materials. Table 2 summarizes the material properties of density, ρ_s, and the volume susceptibility, χ_s, as well as the calculated $B_z \cdot dB_z/dz$ values, which are compared with the experimental $B_z \cdot dB_z/dz$ values obtained from the corresponding levitation positions. Note that for bismuth particles in solid form, the effective values of ρ_s and χ_s measured by the magnetic balance should become smaller in consideration of the measurement setup, consistent with the actual magnetic levitation environment, which includes air between each particle in a test tube. Theoretical $B_z \cdot dB_z/dz$ values were calculated based on equation (3), using the material properties of air as a solvent referred from [29], which gives −879 T^2 m^{-1} for the bismuth particles, and −1376 T^2 m^{-1} for the pure water drop. It was confirmed that the experimental results for the levitation position for each substance with finite size are reasonable from these theoretical assumptions.

5. Numerical simulation results

Figure 7 shows the numerical results of (a) the magnetic field, B_z, and (b) the magnetic field gradient product, $B_z \cdot dB_z/dz$, profiles inside the bore of the HG-TFM (Sim._20 K) and

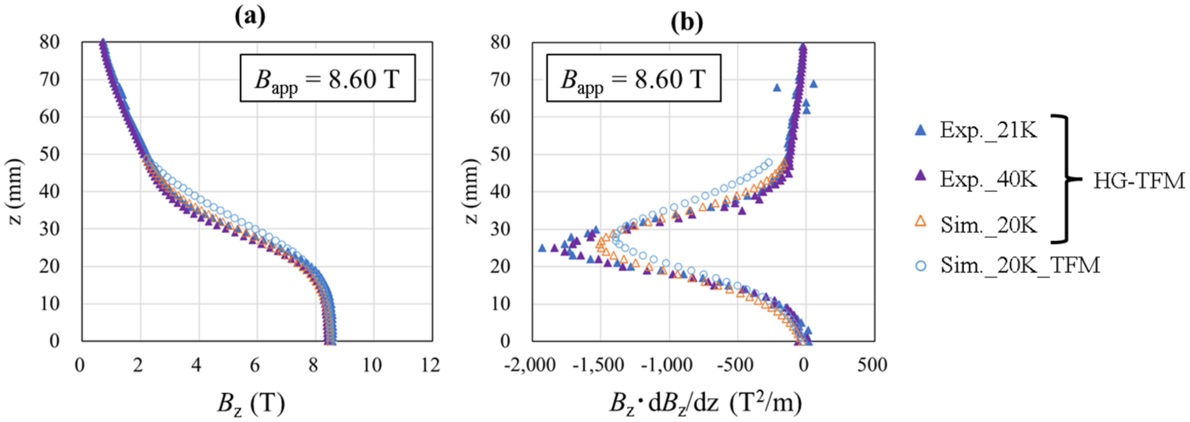

Figure 7. Numerical results of (a) the magnetic field, B_z, and (b) the magnetic field gradient product, $B_z \cdot dB_z/dz$, profiles inside the bore of the HG-TFM and the stacked-TFM along the vertical, z, direction after FCM from $B_{app} = 8.60$ T. The experimental result of the HG-TFM presented in figure 6(a) is labelled as 'Exp._21 K' for comparison. The other experimental result, in which the HG-TFM was magnetized at a higher temperature, $T_{top} = 40$ K, is also given as 'Exp._40 K'.

Table 3. Comparison of magnetic performance, in terms of the trapped field, B_T, and magnetic field gradient product, $B_z \cdot dB_z/dz$, for each case of the HG-TFM and only the TFM, extracted from figure 7.

Case		T (K)	B_T (T)	$B_z \cdot dB_z/dz$ (T^2 m^{-1})
HG-TFM	Exp._21 K	21	8.57	−1930
	Exp._40 K	40	8.39	−1840
	Sim._20 K	20	8.49	−1508
Only TFM	Sim._20 K_TFM	20	8.50	−1397

the stacked-TFM (Sim._20 K_TFM) along the z-direction after FCM from $B_{app} = 8.60$ T at 20 K. For the case of 'Sim._20 K_TFM,' the slit-TFM is considered as air in the model. The experimental result of the HG-TFM presented in figure 6(a) is labelled as 'Exp._21 K' for comparison. The other experimental result, in which the HG-TFM was magnetized at a higher temperature, $T_{top} = 40$ K, is also given as 'Exp._40 K'. As summarized in table 3, a similar magnetic performance could be obtained for the Exp._40 K case magnetized at $T_{top} = 40$ K, but the $B_z \cdot dB_z/dz$ peak as large as -1840 T^2 m^{-1} was equivalent to or a little lower than that at 21 K. In the numerical results of the $B_z \cdot dB_z/dz$ profiles, $B_z \cdot dB_z/dz$ for the Sim._20 K case has a peak value of -1508 T^2 m^{-1} at the same z-position, $z = 25$ mm, as the Exp._21 K case; however, it appears to be much lower than the experimental value. This discrepancy might come from the present 3D modelling, in which the wider slit angle of 6 degrees was employed because of the limitation on the number of mesh elements. Furthermore, the negative magnetic field trapped in the slit-TFM should be explored more in additional experimental studies, to clarify the magnetic performance of each bulk component—the slit-TFM and the full-TFM—separately. Only the case of 'Sim._20 K_TFM' had a peak in a different z-position, $z = 29$ mm, owing to the absence of the slit-TFM, which supports the validity of the hybrid structure of the HG-TFM in the present modelling.

Figure 8 shows the numerical results of (a) the magnetic field, B_z, and (b) the magnetic field gradient product, $B_z \cdot dB_z/dz$, profiles inside the HG-TFM and the stacked-TFM only, after FCM from $B_{app} = 8.60$ T at 20 K. The top schematic views indicate the repulsive, or restoring, magnetic force along the horizontal, xy-plane, presenting the stability along the horizontal plane for a target material levitated in different z-positions. At $z > 30$ mm in the HG-TFM, the B_z profile curves outward and forms a convex-shaped profile along the horizontal plane in the bore, which means a repulsive force would be applied such that the levitated targets collide with a test tube for bismuth particles or the side wall of the vacuum chamber for the water drop, as observed in the experiment. On the other hand, at $z < 30$ mm, the B_z profile forms a concave-shaped profile, where a restoring force would be applied such that the levitated targets remain on the central axis, $x = y = 0$ mm, as depicted in the inset. In a related study of magnetic separation using a conventional SM, reported by Ueda *et al* [30], the magnetic force along the horizontal plane, which differs depending on the height position, is utilized to separate kinds of plastics in an efficient way. In the case of only the stacked-TFM without the negative B_z of the slit-bulk, there is a slight difference 2 mm above, i.e. $z = 32$ mm, with an inflection point that determines the shape of the B_z profiles as convex-, or concave-shaped. Numerical results imply that the levitating state of the targets would be determined by the vector potential of the magnetic force, which differs along the vertical position of the HG-TFM. The reason that both targets could not remain along the central axis as shown in the video comes from a repulsive magnetic force along the horizontal plane in the bore

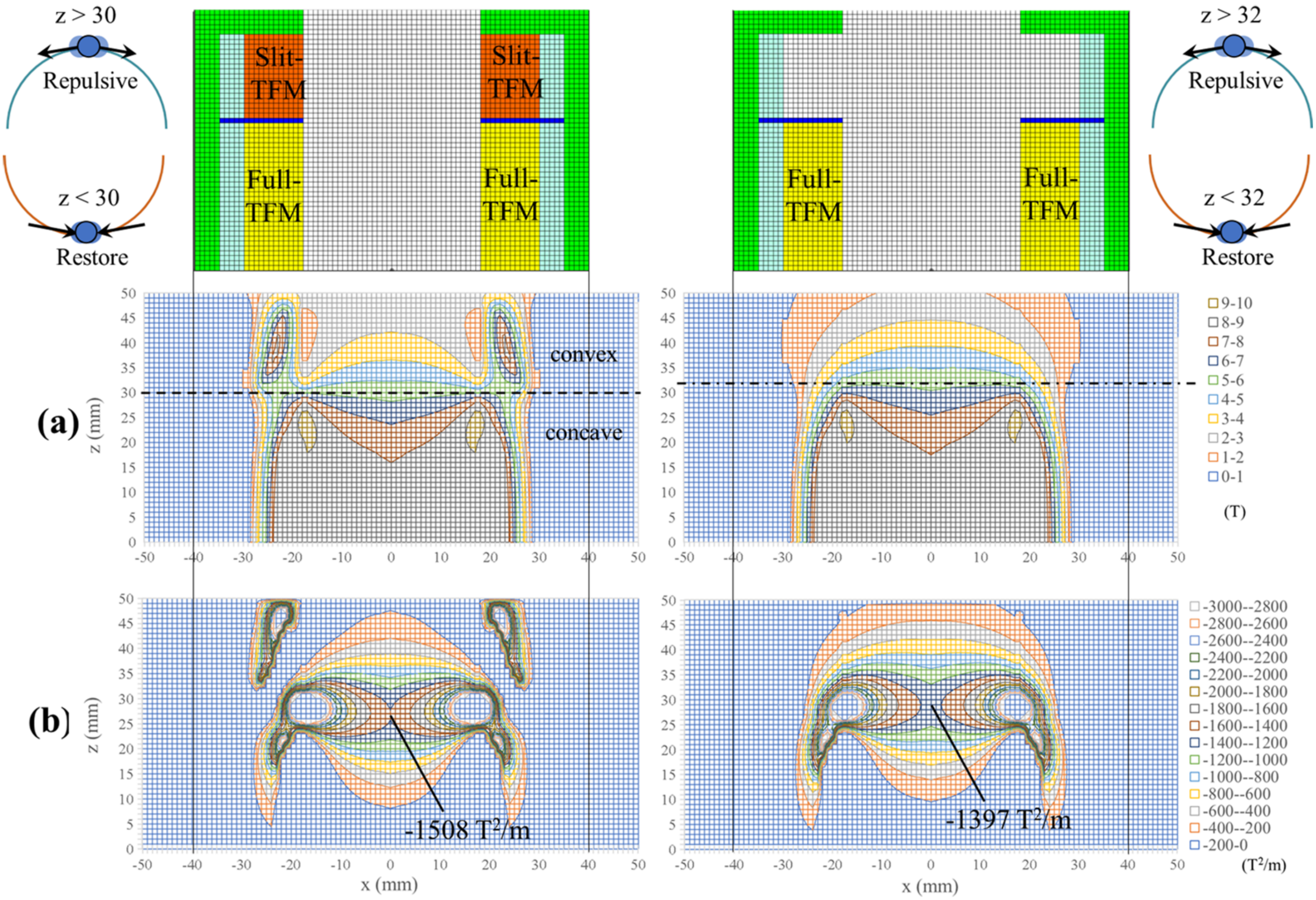

Figure 8. Numerical results of (a) the magnetic field, B_z, and (b) the magnetic field gradient product, $B_z \cdot dB_z/dz$, profiles inside the HG-TFM and the stacked-TFM only, after FCM from $B_{app} = 8.60$ T at 20 K. The top schematic views indicate the repulsive, or restoring, magnetic force along the horizontal, *xy*-plane, describing the stability along the horizontal plane for a target material levitated in different *z*-positions.

of the HG-TFM. One possible recommendation is to avoid such a transition zone between convex-, or concave-shaped profiles at $z = 30$ mm, and levitate target objects statically on the central axis at $z < 30$ mm for the present HG-TFM. The $B_z \cdot dB_z/dz$ profile could be controlled properly, for example, by increasing the operating temperature after magnetization so that the intensity of the $B_z \cdot dB_z/dz$ peak at $z < 30$ mm decreases to the required value for magnetic levitation as calculated by equation (3). The HG-TFM with its superior magnetic capability, $B_z \cdot dB_z/dz = -1508$ T^2 m^{-1}, has an advantage of levitating a wide range of diamagnetic materials, compared to $B_z \cdot dB_z/dz = -1397$ T^2 m^{-1} for the conventional stacked-TFM, as shown in figure 8(b).

The concept of the HG-TFM—including the proposed structure for the cooling and magnetizing process—is validated experimentally, showing that the quasi-microgravity space can be utilized with superior magnetic performance in a room-temperature bore outside the vacuum chamber. These results show that a magnetic field source using bulk superconductors would become an important platform for further applicational studies towards Space Environment Utilization, such as magnetic levitation, magnetic separation, and convection control in a quasi-microgravity.

6. Conclusion

A prototype HG-TFM was built, in which a slit-ring bulk superconductor (slit-TFM) was placed on stacked ring bulks (full-TFM), with the aim of validating the device as a desktop-type magnet, providing a quasi-microgravity space in the room temperature bore of the HG-TFM. Numerical simulation of the trapped field profile in the HG-TFM was also carried out to confirm the validity of the magnetic performance of the HG-TFM measured in the experiment, as well as to explain the mechanism of the levitating state observed in the demonstration of magnetic levitation. The important results and conclusions in this study are summarized as follows.

(a) The present HG-TFM incorporates the slit-bulk TFM and the three stacked full-TFM, all with I.Ds. of 36 mm, which results in a room-temperature bore of 25 mm in diameter and 80 mm in depth. The outer size of the apparatus including the cryocooler is (35 cm × 35 cm) × 103 cm in height.
(b) A trapped field of $B_T = 8.57$ T was achieved at $z = 0$ mm, the bottom of the room temperature bore, after the FCM process from $B_{app} = 8.60$ T at 21.0 K. This resulted in a maximum peak value of the magnetic field gradient

product of $B_z \cdot dB_z/dz = -1930$ T^2 m^{-1} at $z = 25$ mm, the interface of the two bulk components, between the slit-TFM and the full-TFM. During magnetization, the temperatures gradually increased with decreasing external field and the temperature of the top surface of the HG-TFM, T_{top}, took a maximum value of 54.9 K. It was confirmed that a heat sink had a good effect on both the cooling process and the magnetizing process to keep the temperature as low as possible in such stacked TFM cylinders.

(c) The *in-situ* observation of magnetic levitation has validated the quasi-microgravity environment of the HG-TFM for bismuth particles, which floated at $z \cong 35$ mm (± 1 mm): here $B_z \cdot dB_z/dz = -695$ to -950 T^2 m^{-1} and a pure water drop, which floated at $z \cong 30$ mm (± 1 mm): here $B_z \cdot dB_z/dz = -1308$ to -1595 T^2 m^{-1}. It was confirmed that the experimental results for the levitation positions for each substance with finite size are reasonable with theoretical $B_z \cdot dB_z/dz$ values calculated from the material properties of density and magnetic susceptibility.

(d) Numerical simulation results gave a peak value of $B_z \cdot dB_z/dz = -1508$ T^2 m^{-1} at the same z-position, $z = 25$ mm, for the HG-TFM. Only the case of 'Sim._20K_TFM' had a lower peak of $B_z \cdot dB_z/dz = -1397$ T^2 m^{-1} in a different z-position, $z = 29$ mm, owing to the absence of the slit-TFM, which supports the validity of the hybrid structure of the HG-TFM.

(e) It should be noted that the levitating state of the targets would be determined by the vector potential of the magnetic force, which differs along the vertical position of the HG-TFM. As the first step, the magnetic buoyancy force should be applied slowly or step by step to levitate stably at a constant vertical position, as observed for the bismuth particles. This is difficult for a pure water drop in liquid form as it is. Furthermore, regarding to the horizontal direction, a repulsive magnetic force would be applied with a convex-shaped magnetic profile at $z > 30$ mm such that the levitated targets collide with a test tube or the side wall of the vacuum chamber as observed, while the restoring magnetic force would be applied with a concave-shaped profile at $z < 30$ mm in contrast.

Data availability statement

The data that support the findings of this study are openly available at the following URL/DOI: https://doi.org/10.17863/CAM.80920.

Acknowledgments

A portion of this research was supported from JSPS Fellows Grant No. 21J14069, as well as from JSPS KAKENHI Grant No. 19K05240, and from Adaptable and Seamless Technology transfer Program through Target-driven R&D (A-STEP) from Japan Science and Technology Agency (JST), Grant No. JPMJTM20AK.

M D Ainslie would like to acknowledge financial support from an Engineering and Physical Sciences Research Council (EPSRC) Early Career Fellowship, EP/P020313/1.

ORCID iDs

Keita Takahashi https://orcid.org/0000-0002-8278-2688
Hiroyuki Fujishiro https://orcid.org/0000-0003-1483-835X
Mark D Ainslie https://orcid.org/0000-0003-0466-3680

References

[1] McPherson A and DeLucas L J 2015 Microgravity protein crystallization *npj Microgravity* **1** 15010

[2] Imura T, Nakagawa K, Kawahara Y and Yuge L 2018 Stem cell culture in microgravity and its application in cell-based therapy *Stem Cells Dev.* **27** 1298–302

[3] Durmus N G, Tekin H C, Guven S, Sridhar K, Arslan Yildiz A, Calibasi G, Ghiran I, Davis R W, Steinmetz L M and Demirci U 2015 Magnetic levitation of single cells *Proc. Natl Acad. Sci. USA* **112** E3661–8

[4] Robinson J A, Rhatigan J L, Baumann D K, Tate J and Thumm T 2006 International space station research summary through expedition 10 *NASA/TP*-2006-213146 (NASA Technical Publication)

[5] Ando T, Hirota N and Maie M 2015 Development of recovery device for particulates in fluid by magneto-Archimedes separation *Sep. Purif. Technol.* **149** 197–207

[6] Houlton J, Chen M, Brubaker M, Bertness K and Rogers C 2018 Axisymmetric scalable magneto-gravitational trap for diamagnetic particle levitation *Rev. Sci. Instrum.* **89** 125107

[7] Ikezoe Y, Kaihatsu T, Sakae D, Uetake H, Hirota N and Kitazawa K 2002 Separation of feeble magnetic particles with magneto-Archimedes levitation *Energy Convers. Manage.* **43** 417–25

[8] Watanabe K, Takahashi K, Mogi I, Nishijima G, Awaji S and Motokawa M 2003 Cryogen-free hybrid magnet for magnetic levitation *Physica* C **386** 485–9

[9] Subramaniam A B, Yang D, Yu H-D, Nemiroski A, Tricard S, Ellerbee A K, Soh S and Whitesides G M 2014 Noncontact orientation of objects in three-dimensional space using magnetic levitation *Proc. Natl Acad. Sci. USA* **111** 12980–5

[10] Miura O, Yamagishi K and Yamamoto D 2018 Magneto-Archimedes levitation of precious metals under a high magnetic field gradient *J. Phys.: Conf. Ser.* **1054** 012086

[11] Kobayashi T, Mori T, Akiyama Y, Mishima F and Nishijima S 2017 Study on separation of structural isomer with magneto-Archimedes method *J. Phys.: Conf. Ser.* **897** 012018

[12] Bean C P 1962 Magnetization of hard superconductors *Phys. Rev. Lett.* **8** 250

[13] Bean C P 1964 Magnetization of high-field superconductors *Rev. Mod. Phys.* **36** 31

[14] Durrell J H *et al* 2012 A trapped field of >3 T in bulk MgB_2 fabricated by uniaxial hot pressing *Supercond. Sci. Technol.* **25** 112002

[15] Durrell J H *et al* 2014 A trapped field of 17.6 T in melt-processed, bulk Gd-Ba-Cu-O reinforced with shrink-fit steel *Supercond. Sci. Technol.* **27** 082001

[16] Huang K *et al* 2020 Composite stacks for reliable >17 T trapped fields in bulk superconductor magnets *Supercond. Sci. Technol.* **33** 02LT01

[17] Takahashi K, Fujishiro H and Ainslie M D 2018 A new concept of a hybrid trapped field magnet lens *Supercond. Sci. Technol.* **31** 044005
[18] Takahashi K, Fujishiro H, Namba S and Ainslie M D 2021 Experimental realization of an all-(RE)BaCuO hybrid trapped field magnet lens generating a 9.8 T concentrated magnetic field from a 7 T external field *Supercond. Sci. Technol.* **34** 05LT02
[19] Takahashi K, Fujishiro H and Ainslie M D 2021 A conceptual study of a high gradient trapped field magnet (HG-TFM) toward providing a quasi-zero gravity space on Earth *Supercond. Sci. Technol.* **34** 035001
[20] Fujishiro H and Naito T 2011 Simulation of temperature and magnetic field distribution in superconducting bulk during pulsed field magnetization *Supercond. Sci. Technol.* **23** 105021
[21] Fujishiro H, Ainslie M D, Takahashi K, Naito T, Yanagi Y, Itoh Y and Nakamura T 2017 Simulation studies of mechanical stress in REBaCuO superconducting ring bulks with infinite and finite height reinforced by metal ring during field-cooled magnetization *Supercond. Sci. Technol.* **30** 085008
[22] Takahashi K, Fujishiro H, Naito T, Yanagi Y, Itoh Y and Nakamura T 2017 Fracture behavior analysis of EuBaCuO superconducting ring bulk reinforced by a stainless steel ring during field-cooled magnetization *Supercond. Sci. Technol.* **30** 115006
[23] Ainslie M D and Fujishiro H 2015 Modelling of bulk superconductor magnetization *Supercond. Sci. Technol.* **28** 053002
[24] Ainslie M D and Fujishiro H 2019 *Numerical Modelling of Bulk Superconductor Magnetization. IOP Expanding Physics* (Bristol: IOP Publishing)
[25] Jirsa M, P̊ust L, Dlouhý D and Koblischka M R 1997 Fishtail shape in the magnetic hysteresis loop for superconductors: interplay between different pinning mechanisms *Phys. Rev.* B **55** 3276–84
[26] Kii T *et al* 2012 Low-temperature operation of a bulk HTSC staggered array undulator *IEEE Trans. Appl. Supercond.* **22** 4100904
[27] Muralidhar M, Sakai N, Jirsa M and Koshizuka N 2004 Direct observation and analysis of nanoscale precipitates in (Sm, Eu, Gd)$Ba_2Cu_3O_y$ *Appl. Phys. Lett.* **85** 3504
[28] Takahashi K, Fujishiro H and Ainslie M D 2020 Simulation study for magnetic levitation in pure water exploiting the ultra-high magnetic field gradient product of a hybrid trapped field magnet lens (HTFML) *J. Appl. Phys.* **127** 185106
[29] Schenck J F 1996 The role of magnetic susceptibility in magnetic resonance imaging: MRI magnetic compatibility of the first and second kinds *Med. Phys.* **23** 815–50
[30] Ueda Y, Mishima F, Akiyama Y and Nishijima S 2014 Fundamental study of plastic separation utilizing magnetic force *IEEE Trans. Appl. Supercond.* **24** 3700805